Interaction and Multiscale Mechanics, Vol. 1, No. 4 (2008) 437-448
DOI: http://dx.doi.org/10.12989/imm.2008.1.4.437

Dislocation dynamics simulation on stability of high dense dislocation structure interacting with coarsening defects

M. Yamada, T. Hasebe* and Y. Tomita

Graduate School of Engineering, Kobe University, 1-1 Rokkodai, Nada, Kobe, 657-8501, Japan

T. Onizawa

Japan Atomic Energy Agency, Core and Structural Group, Advanced Nuclear System Research and Development Directorate, 4002 Narita, O-arai, Ibaraki 311-1393, Japan

(Received March 25, 2008, Accepted November 24, 2008)

Abstract. This paper examined the stability of high-dense dislocation substructures (HDDSs) associated with martensite laths in High Cr steels supposed to be used for FBR, based on a series of dislocation dynamics (DD) simulations. The DD simulations considered interactions of dislocations with impurity atoms and precipitates which substantially stabilize the structure. For simulating the dissociation processes, a point defect model is developed and implemented into a discrete DD code. Wall structure composed of high dense dislocations with and without small precipitates were artificially constructed in a simulation cell, and the stability/instability conditions of the walls were systematically investigated in the light of experimentally observed coarsening behavior of the precipitates, i.e., stress dependency of the coarsening rate and the effect of external stress. The effect of stress-dependent coarsening of the precipitates together with application of external stress on the subsequent behavior of initially stabilized dislocation structures was examined.

Keywords: dislocation dynamics; dislocation substructure; creep strength; high Cr steel; multiscale modeling; field theory.

1. Introduction

The key feature of high Cr steels possessing excellent high temperature creep strength is attributed largely to the hierarchically introduced complex microstructures composed of high dense dislocation structures in the lath martensite, lath blocks and the packets extending multiple scales (Muruyama *et al.* 2001). The creep strength of such high Cr steels, however, has been reported to be rapidly deteriorated exceeding 100,000 hrs under some accelerated conditions presumably due to inhomogeneous recovery of the lath structures (Kushima *et al.* 1999). Since the steels are expected to be used for fast-breeder reactor (FBR), whose lifetime is supposed to be over 50,000hrs during

* Corresponding Author, E-mail: hasebe@mech.kobe-u.ac.jp

which the plant cannot be frequently started-up and shut-down, an appropriate as well as accurate method for the creep-fatigue damage evaluation is urgently required (Kimura *et al*. 2003).

The strength of the lath martensite structure is essentially controlled by the associated high dense dislocation structures (HDDSs, hereafter). The HDDSs are normally stabilized with a strong help of interstitial atoms as well as small carbides. Therefore, the stability/instability of the HDDSs would be the most important ingredient ultimately controlling the strength of the steels. It has been experimentally observed that the inhomogeneous recovery of the lath structures taken place under relatively small stress level results in significant reduction of the creep strength. The detailed mechanisms and the quantitative controlling factors, however, have not been clarified to date because of the complexity of the microstructures as well as the series of processes itself.

The ultimate goal of the present study is to develop simulation models for the deterioration processes of the complex microstructure in high Cr steels in several representative scale levels, and to propose a practically feasible damage evaluation method in conjunction with the field theory of plasticity (Hasebe 2004a, 2004b). The representative scales in the present context are (A) lath martensite, (B) lath block and (C) lath packet structures as schematically illustrated in Fig. 1, where the degraded counterparts are also illustrated mainly due to the collapse of HDDSs in the scale A.

In this paper, we perform the smallest scale simulations the corresponding to the above scale A by utilizing a discrete dislocation (DD) model and discusses the stability/instability characteristics of HDDSs which mimic those composing the lath martensite structures. A defect model based on the analytical solution for the interaction with a straight dislocation is developed and implemented into a DD code (MDDP-suite: Multiscale Dislocation Dynamics Plasticity (Zbib 2002)). Stability of an artificially-constructed wall structure composed of high dense dislocation networks is extensively discussed based on a series of simulations with and without precipitates and external stress. Stress dependent coarsening of the precipitates is also taken into account and its effects on the wall stability is further examined.

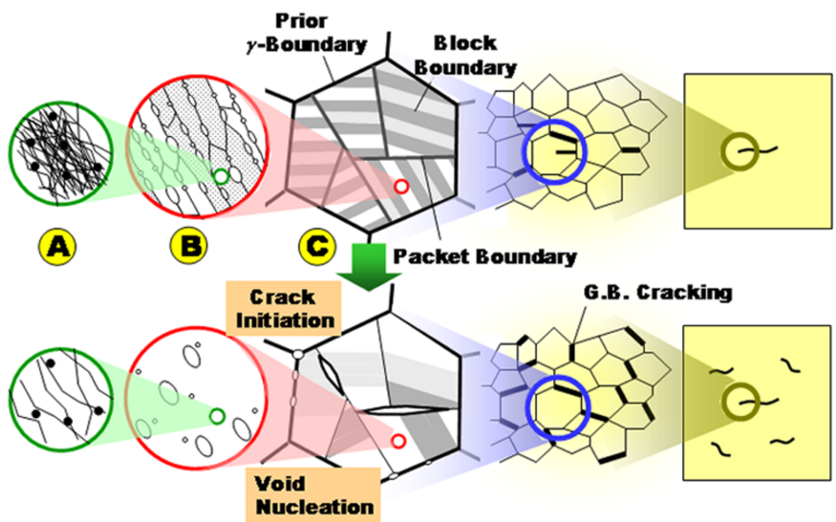

Fig. 1 Schematics of multiscale microstructure of high Cr ferretic steel composed of high dense dislocation structure (HDDS) in lath martensite, lath block and lath packet structures, together with deteriorates counterparts due to inhomogeneous recovery under creep

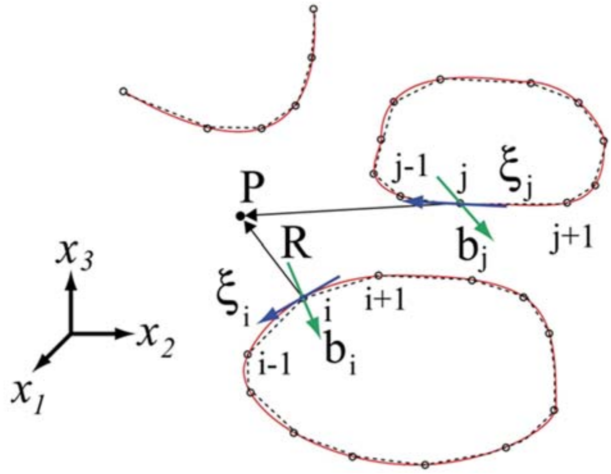

Fig. 2 Nodes and segments on dislocation loops

2. Simulation procedure

2.1 Outline of discret dislocation method

Discrete Dislocation Dynamics (DDD) code developed by Zbib (Zbib *et al*. 1998, Zbib 2002) is a method to chase the behavior of individual dislocations by discretizing them into straight segments on which forces are evaluated to calculate stress field. One of the advantages of the scheme over the others (Kubin *et al*. 1992, Ghoniem *et al*. 1999) is the ease of implementation of local rules as junction formation and cross slip by virtue of the segment-based formalism. In this paper, we will implement a defect model for precipitates into the code by making the use of this feature.

The stress at *P*, as schematized in Fig. 2, is analytically given by.,

$$\sigma_{\alpha\beta}(P) = -\frac{\mu}{8\pi}\oint_c b_m \in_{im\alpha}\frac{\partial}{\partial x'_i}\nabla'^2 R dx'_\beta - \frac{\mu}{8\pi}\oint_C b_m \in_{im\beta}\frac{\partial}{\partial x'_i}\nabla'^2 R dx'_\alpha$$
$$-\frac{\mu}{4\pi(1-\nu)}\oint_c b_m \in_{imk}\left(\frac{\partial^3 R}{\partial x'_i \partial x'_\alpha \partial x'_\beta} - \delta_{\alpha\beta}\frac{\partial}{\partial x'_i}\nabla'^2 R\right) dx'_k \quad (1)$$

where b_i is the magnitude of the Burgers vector, μ is the share modulus, ν is Poisson's rate, R is the distance between P and a dislocation segment, and $\in_{ijk}$ is the permutation symbol. Discretized version of Eq. (1) for stress field representation is,

$$\sigma_{\alpha\beta}(P) = \sum_{all\ Loops} \sum_{j=1}^{n-1}\left\{-\frac{\mu}{8\pi}\int_j^{j+1} b_m \in_{im\alpha}\frac{\partial}{\partial x'_i}\nabla'^2 R_j dx'_\beta - \frac{\mu}{8\pi}\int_j^{j+1} b_m \in_{im\beta}\frac{\partial}{\partial x'_i}\nabla'^2 R_j dx'_\alpha\right.$$
$$\left.-\frac{\mu}{4\pi(1-\nu)}\int_j^{j+1} b_m \in_{im\alpha}\left(\frac{\partial^3 R_j}{\partial x'_i \partial x'_\alpha \partial x'_\beta} - \delta_{\alpha\beta}\frac{\partial}{\partial x'_i}\nabla'^2 R_j\right) dx'_k\right\} \quad (2)$$

where R_j represents the distance between P and a dislocation node j, while n is the number of nodes included in a dislocation line or loop.

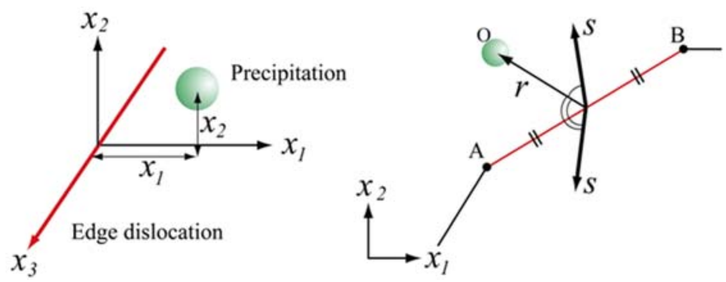

Fig. 3 Straight edge dislocation and precipitate model

2.2 Simulation model

2.2.1 Defect model for precipitates

Elastic interaction energy E_{int} between a straight edge dislocation and a spherical defect, as illustrated in Fig. 3, is given as (Kato 1999),

$$E_{\text{int}} = -V\mu b\varepsilon \frac{(1+\nu)}{\pi(1-\nu)}\left(\frac{x_2}{x_1^2+x_2^2}\right) \tag{3}$$

where V and ε are the volume and strain of the defect, respectively (Hirth & Lothe 1992). One can obtain the force acting on the dislocation by the partial differentiation of E_{int} with respect to x_1, i.e.,

$$F = -\frac{\partial E_{\text{int}}}{\partial x_1} = -V\mu b\varepsilon \frac{(1+\nu)}{\pi(1-\nu)}\left[\frac{2x_1x_2}{(x_1^2+x_2^2)^2}\right] \tag{4}$$

If x_2 is constant, F is in inversely proportional to the cube of x_1. In this paper, we assume that F is in proportion to the distance considering the interaction between an edge dislocation and a spherical precipitate. Therefore, we have,

$$F = \lambda\frac{A}{|r|^3}, \qquad \lambda = \frac{r\cdot s}{|r\cdot s|} \tag{5}$$

where A is a parameter measuring the strength of precipitate, while r is distance vector, and s is unit velocity vector of dislocation segment. Here λ expresses the sign of the force from the precipitate concerned: If a precipitate model expresses that generates repulsive force, λ is positive as dislocation approaches, whereas it turns to negative after the precipitate is passed over.

2.2.2 Dislocation model

Fig. 4 shows a schematic of a dislocation wall as a model of high dense dislocation structures (HDDSs) composing lath martensite in high Cr steels, artificially constructed .in a simulation cell with side lengths of 0.25 μm. The wall model is composed of two sets of straight dislocations along [100] and [001] directions which respectively belong to (011) $[11\bar{1}]$ and (011) $[\bar{1}1\bar{1}]$ slip systems. The former will be mentioned as "wall 1," while the latter "wall 2." Each wall has 10 dislocation lines, therefore the total number of the wall constructing dislocations is 20, leading the initial dislocation density of 3.239×10^{14} $[m/m^3]$

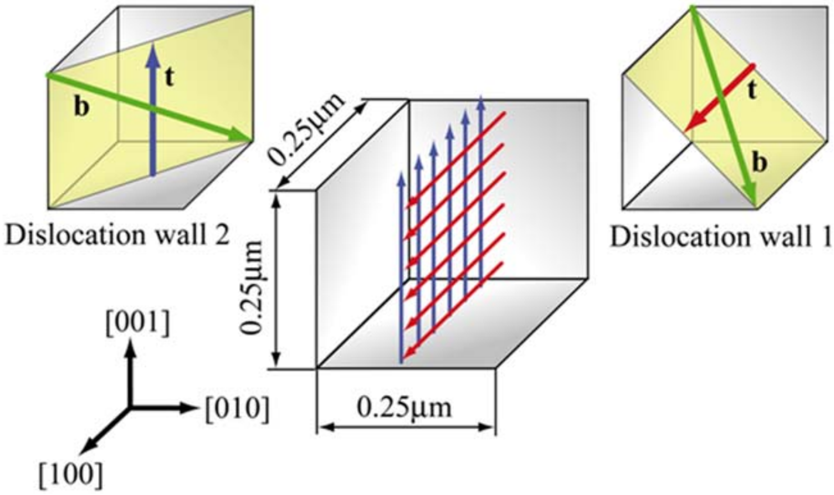

Fig. 4 Dislocation wall model and its settings

Table 1 Material constants used in DD simulations

Shear modulus [GPa]	85.4
Density [kg/m^3]	7630
Poisson ratio	0.279
Magnitude of Burgers vetor [m]	2.485×10^{-10}

2.3 Simulation conditions

Material to be simulated is Fe having BCC structure. The material constants used are listed in Table 1. Roughly two situations are examined, i.e., (1) with and without precipitate models, and (2) with and without application of external stress. The condition without both the precipitate model and external stress is thus regarded as a reference. For the case with the precipitate model, the total number of precipitates is set to 200 as an initial condition, which provides the volume fraction of 1.047×10^{-3} and mean spacing of 5.57×10^{-2} μm. For the external stress, $\sigma_{11} = \sigma_{33} = -100$ [MPa] is applied considering Peach-Koehler force acting on the walls 1 and 2 to drive them in the opposite direction. Peach-Koehler force par unit length is given by

$$\frac{\boldsymbol{F}_{gl}}{\boldsymbol{L}} = \frac{[(\boldsymbol{b} \cdot \boldsymbol{\sigma}) \times \xi] \cdot [\xi \times (\boldsymbol{b} \times \xi)]}{|\boldsymbol{b} \times \xi|} \tag{7}$$

where ξ represents the line direction of a dislocation segment.

Also, a preliminary analysis is made to determine the parameters employed in the precipitate model in terms of strength and size of the defect assumed in this study. We simulated a process of Orowan loop formation and evaluate the Orowan stress. Simulation set up is shown in Fig. 5. A straight edge dislocation is placed on (011) slip plane in a simulation cell with side lengths of 0.28mm, whereas five precipitates are situated with a mean spacing set in the above. Constant external shear stress $\sigma_{31} = 450$ MPa is applied in the normal direction to the dislocation line.

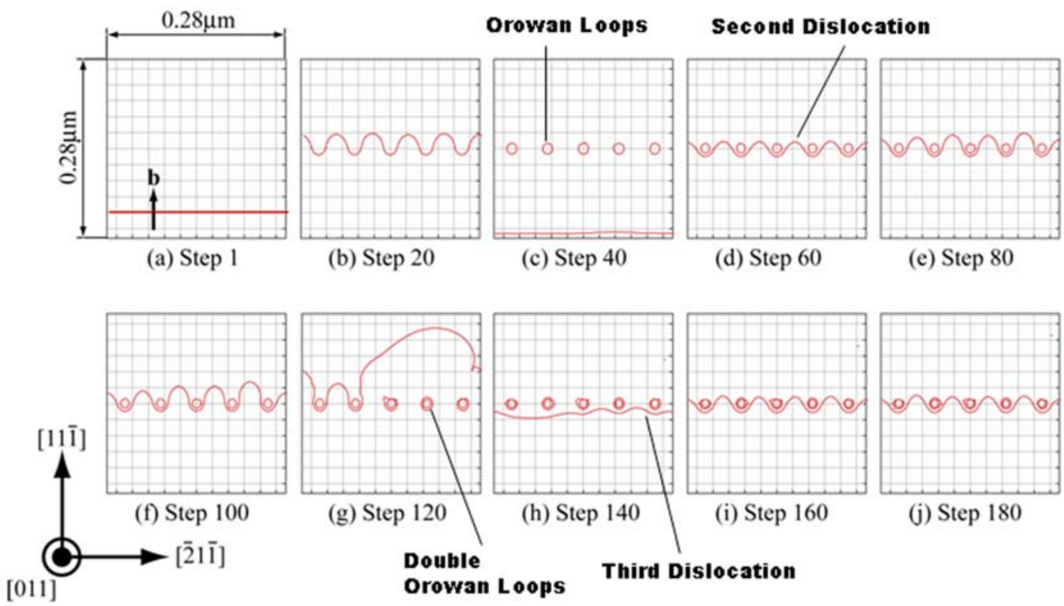

Fig. 5 Preliminary simulation result for moving edge dislocations interacted with precipitate models introduced, demonstrating Orowan loop formations

3. Results and disscutions

3.1 Orowan loop formation and Orowan stress

Theoretical value of the Orowan stress is given by,

$$\tau_{OR} = \frac{\mu b}{L} \tag{8}$$

where L is the mean spacing of precipitates. In the present case, we have $\tau_{OR} = 381$ MPa.

Fig. 5 shows an example of the simulation results demonstrating Orowan loop formations and associated bowing-out behavior of dislocation lines. Bowing-out of the first dislocation line leaving behind single Orowan loops is seen in (b) and (c), while the subsequent passing of another dislocation results in double Orowan loop formation as in (d) through (h). Further bowing-out is restricted because of the elevated Orowan stress based on the above processes as can be seen in (i) and (j).

Based on evaluation of the critical value for the force overcoming the precipitates leaving Orowan loops, i.e., the Orowan stress, we determined the parameter A to be 7.25×10^9 N/m^3. Note, in addition to precipitates, the present model can mimic basically any kinds of defects, for example, small point defect like solute atoms of interstitial type and large defects like volume defects, with both attractive and repulsive interactions with dislocations.

3.2 Behavior of dislocation model and its stability

Fig. 6(a) shows a referential result, i.e., with neither precipitate model nor external stress. As can

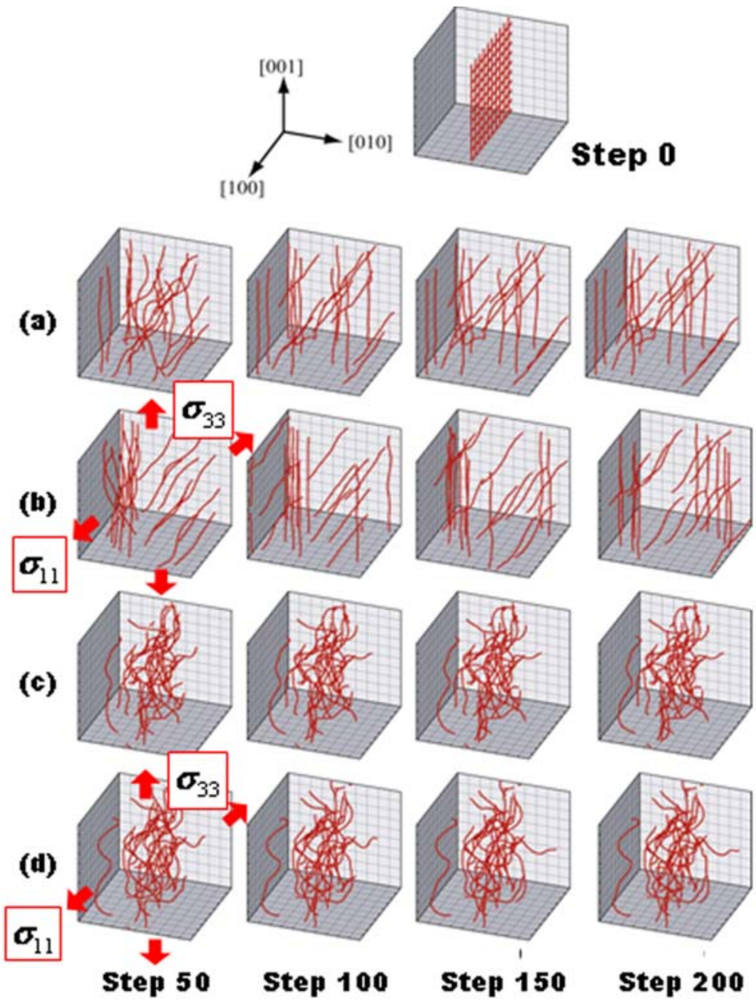

Fig. 6 Snapshots of collapsing wall structure with and without defect model. (a) without stress and precipitate, (b) with stress with no precipitate, (c) without stress but with precipitates (N = 200) and (d) with both external stress and precipitates

be confirmed, the wall structure collapses in the absence of both precipitates and external stress. The structure is fully dissociated and reaches a near-equilibrium configuration at around 150 time steps. The application of external stress accelerates the collapse and tends to lead the system to another equilibrium configuration as seen in Fig. 6(b).

Fig. 6(c) shows the result with randomly distributed precipitates (N = 200: not indicated). Distributing the precipitates is demonstrated to be able to pin the wall-constructing dislocations effectively, resulting in aggregation of tangled dislocation cluster reconstructed near the center of the simulation cell. The pinned structure remains almost stable even under external stress as shown in Fig. 6(d), although some segments lying between pair of precipitates bowed out and changed their configurations slightly. These results imply that the stability of wall structures can be controlled by introducing distributing precipitates as one can intuitively imagine and understand.

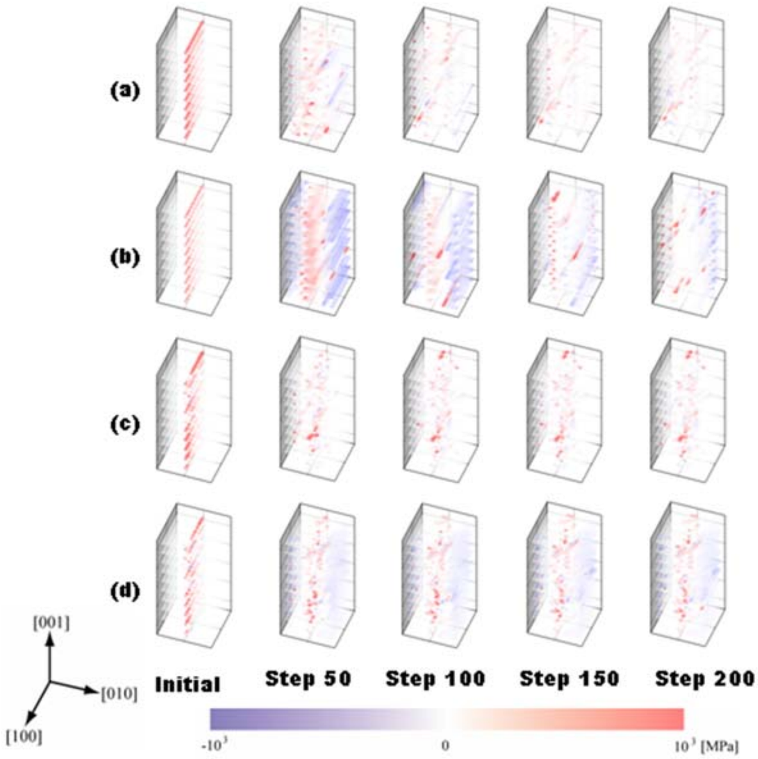

Fig. 7 Snapshots of distribution of σ_m with and without defect model corresponding to Fig. 5. (a) without stress and precipitate, (b) with stress with no precipitate, (c) without stress but with precipitates (N = 200) and (d) with both external stress and precipitates

Corresponding stress distributions to Fig. 6 are given in Fig. 7, where the hydrostatic component is chosen as an example. The figure depicts overlaying [100]-[010] in-plane contour diagrams along [001] direction. The referential case without precipitate and external stress (Fig. 7(a)) yields rapid spread of the stress over the simulation cell reaching ultimately the equilibrium state. Fig. 7(c), i.e., the case with randomly distributed 200 precipitates, on the other hand, shows stagnating hydrostatic stress distribution in the central region of the simulation cell, corresponding to the tangled dislocations thereabout shown in Fig. 6(c). The biased hydrostatic stress distribution produces large stress gradient, which may be the key to evaluate the structural stability of the HDDSs.

The above results clearly demonstrate the effectiveness of the presently proposed defect model coupled with DD simulations for investigating the stability of HDDSs, which allows us, e.g., parametric type of simulations with different type, number, distribution, and size of defects as well as external stress conditions.

3.3 Effect of coarsening precipitates

Coarsening of some kinds of carbides like $M_{23}C_6$ has been reported to be accelerated with a help of stress. This paper also studies the effect of such stress dependency of the coarsening behavior of precipitates on the HDD wall stability. The coarsening due to the Ostward ripening has been

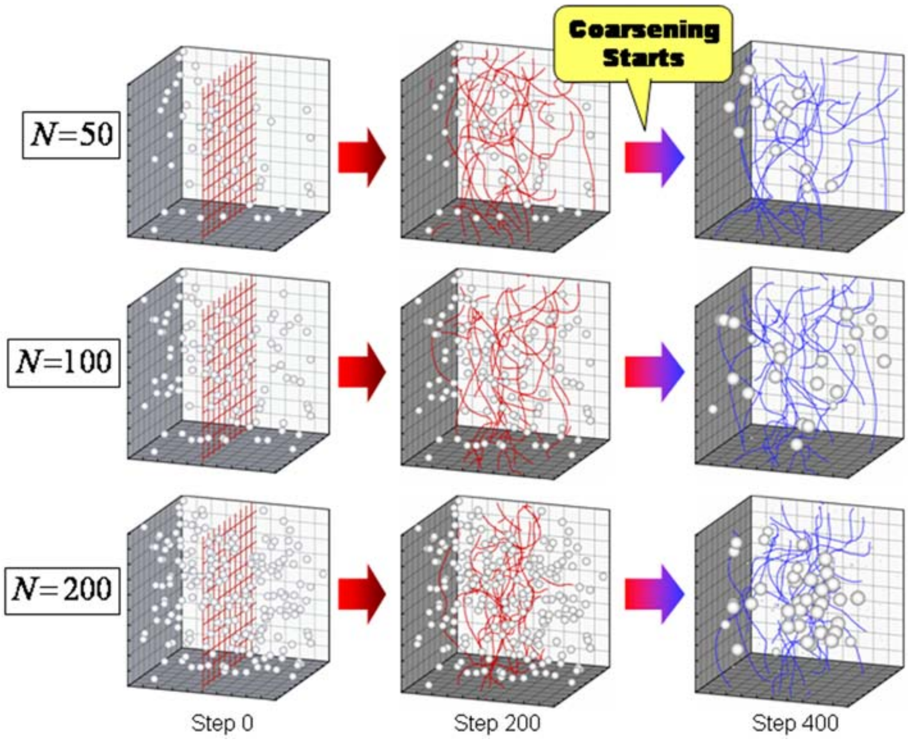

Fig. 8 Effect of initial number of precipitates on stability of HDDSs comparing three cases, i.e., N = 50, 100 and 200. Relaxed configurations after 20 simulation time steps are used as initial states, after when stress-dependent coarsening of precipitates start to operate

reported to take place in the present material during creep (e.g. Taneike *et al*. 2001). Here we introduce a phenomenological model for the coarsening process simply given as a function of a stress measure. Since the detailed mechanism of the stress-assisted coarsening has not been well-documented, the coarsening law is assumed here to be expressed in terms of the rate of the radius change, i.e.,

$$\dot{r} = \dot{r}_0 \tanh\left(\frac{\sigma_{mes}}{\langle \sigma_{mes} \rangle} - 1\right) \tag{9}$$

where σ_{mes} expresses the stress measure responsible for the stress dependent coarsening evaluated at the center of each precipitate, and $\langle \sigma_{mes} \rangle$ is the spatial mean value of σ_{mes} for all the precipitates in the simulation cell. The present study tentatively employs hydrostatic stress σ_m (identical to the stress invariant J_1) for the stress measure, i.e., $\sigma_m = \sigma_{mes}$ and $\langle \sigma_{mes} \rangle = \langle \sigma_m \rangle$ as a first step, because it takes both positive and negative values together with a clear physical image. Other possibilities would be the rest of the stress invaria nts, i.e., J_2 and J_3, where the former corresponds to equivalent stress but only takes positive value, while the latter yield no clear physical meaning although it can also take both signs.

We consider three cases with different numbers of initially-introduced precipitates, i.e., N = 50, 100 and 200. Fig. 8 shows the initial configurations of the precipitates together with wall-constructing dislocations. The initial diameter of the precipitates is set to be 25 nm, being commensurate with that of MX-type carbonitrides, which is kept constant until 200 simulation steps.

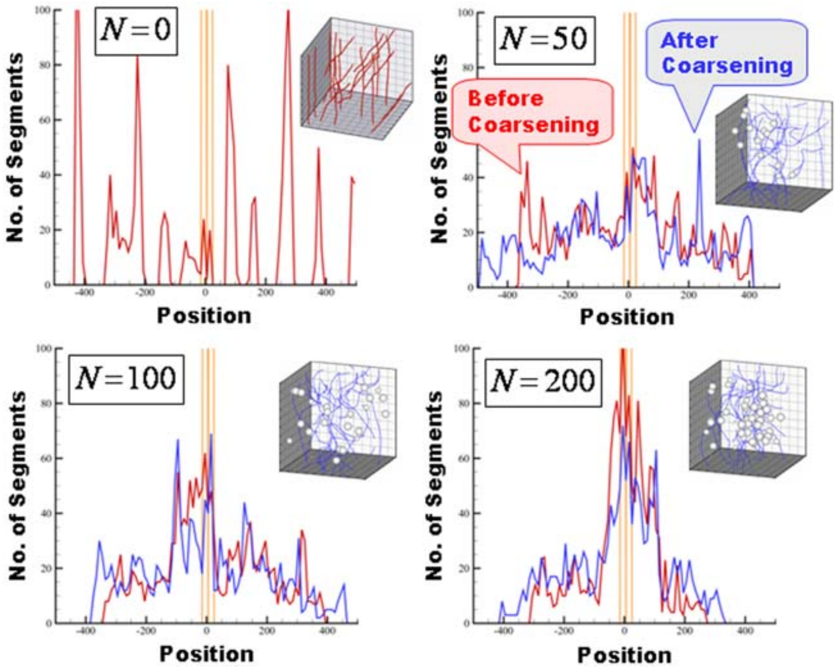

Fig. 9 Quantitative comparison of results in Fig. 8 indicating dislocation segment distributions before and after coarsening

A quasi-equilibrium state of dislocations is reached at 200 steps, at which the precipitates are started to coarsen according to Eq. (9). Fig. 8(c) shows final configurations of the coarsened precipitates and entangled dislocations around them. Since no external stress is applied in these cases, the coarsening is solely due to the internal stress field produced by the dislocations themselves. As is expected, larger number of initially-introduced precipitates results in more stable final configuration of HDDSs. In other words, as the number of initial precipitates increases, the stability of HDDSs becomes less sensitive to the coarsening process itself.

Fig. 9 compares the distribution of dislocation segments for the results presented in Fig.8 representing the change of the dislocation distribution. The number of segments of dislocations in the regions parallel to the initial wall ((010) plane) are summed over and projected on to the perpendicular plane ((100) plane). Two straight lines in the central region correspond to the initial wall positions. For comparison, the result without precipitate is also shown. The segment distribution in this case yields many sharp peaks almost independent each other, meaning the dislocations tend to stay straight (not curved) essentially free from stress acting on the dislocation lines. In sharp contrast, the other cases with precipitates, the segment distributions are continuous reflecting stressed and thus curved dislocation lines. In the case of $N = 50$, we observe nearly uniformly redistributed dislocation segments at the end with an isolated peak near the right edge of the simulation cell, implying the dislocation structure is fully collapsed as a consequence of the coarsening, whereas the other two cases more or less retain the continuity in the segment distributions. In particular, the $N = 200$ case maintains exclusively sharp peak at the center even after the coarsening is terminated. There observes relatively small difference in the distributions between that at the outset of coarsening and the final state. This means that the structure is stable. We employ the $N = 200$ case in the following to examine the effect of external stress.

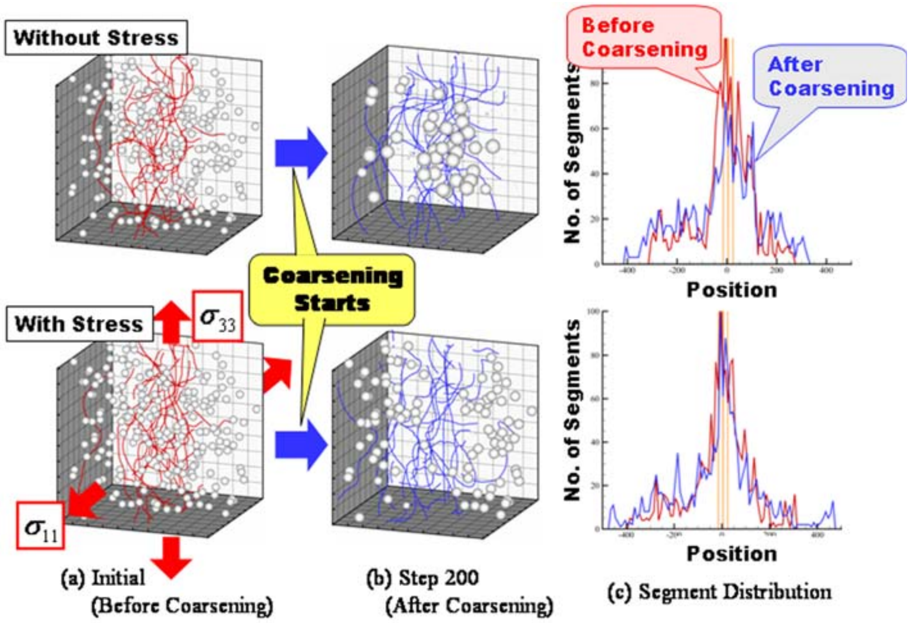

Fig. 10 Effect of external stress on stability of HDDSs for N = 200 precipitates considering stress-dependent coarsening

Fig. 10 compares the coarsening processes and concomitant collapsing behavior of HDDSs between that under external stress and the stress free condition for N = 200. The 200 simulation time steps for both the cases, similarly to the above, are regarded again as the initial configuration of HDDSs, at which the coarsening is set to start. Clear difference can be found between the two cases. Namely, without external stress, non-uniform coarsening takes place and the coarsened precipitates are segregated to the central region of the simulation cell. Application of external stress, on the other hand, tends to promote rather uniform coarsening with smaller final size of the precipitates compared with the other case, and the resultant distribution tends to sandwich the clustered dislocations. Both the cases resultantly have similar dislocation configurations but with totally opposite precipitate distributions, i.e., the former yield relatively smaller number of fairly coarsened precipitates clustered around the dislocation aggregate in the central region, whereas the latter exhibits moderately coarsened many precipitates relatively uniformly distributed over the simulation cell and sandwiching the dislocation aggregate. These results imply a paradoxical effect of the application of external stress which rather restricts the inhomogeneous coarsening of the initially-introduced precipitates, and consequently, the recovery of the HDDSs.

The above results demonstrate the significant contribution of the field fluctuation rather than the magnitude of the externally-applied stress to the non-uniformity or inhomogeneity in the coarsening behaviors of precipitates, implying that $\delta\sigma_{mes}/\sigma_{mes}$ should be considered instead of $\delta\sigma_{mes}$ or σ_{mes} alone as the measure. This interpretation is consistent with the experimentally observed trend in terms of recovery of the microstructure (Kushima *et al.* 1999, 2003), where smaller stress levels yield more rapid and clear degradation of creep strength due to inhomogeneous recovery of the lath structures, whereas larger external stresses tend to result in the creep rupture times commensurate with those predicted via Larson-Miller parameter, stemming from the uniform recovery of the microstructure. Since the fluctuation component of stress comes not only from the composing dislocations themselves but from the upper scale inhomogeneities as intra- and trans-granular levels, the next step of this study is to systematically examine the effect of those "external" stress fluctuations.

4. Conclusions

This paper examined the stability of high-dense dislocation substructures (HDDSs) associated with martensite laths in High Cr steels based on dislocation dynamics (DD) simulations. A simplified defect model which can mimic impurity atoms and precipitates was proposed and implemented into a DD code to take into account the interactions with dislocations. A wall structure composed of a pair of straight dislocation arrays was considered as an example of the HDDSs. The effect of stress-dependent coarsening of the precipitates together with application of external stress on the subsequent behavior of initially stabilized dislocation structures were extensively examined in terms of changes in the internal stress field, where hydrostatic stress distribution was taken as an example. Application of stress was shown to promote rather uniform recovery (coarsening) than that without stress, resulting in comparably stable HDDSs.

References

Ghoniem, N. M. and Sun, L. Z. (1999), "Fast-sum method for the elastic field of three-dimensional dislocation ensembles", *Phys. Rev.*, **B60**, 128-140.

Ghoniem, N. M., Tong, S. -H. and Sun, L. Z. (1999), "Parametric dislocation dynamics: A thermodynamics-based approach to investigations of mesoscopic plastic deformation", *Phys. Rev.*, **B61**, 913-927.

Hasebe, T. (2004a), "Field theoretical multiscale polycrystal plasticity", *Trans. MRS-J*, **29**, 3619-3624.

Hasebe, T. (2004b), "Continuum description of inhomogeneously deforming polycrystalline aggregate based on field theory", in H. Kitagawa, Y. Shibutani eds. *Mesoscopic Dynamics of Fracture Process and Materials Strength*, *IUTAM Symp.*, 381-390, Kluwer.

Hasebe, T. (2006), "Multiscale crystal plasticity modeling based on field theory", *CMES*, **11**-3, 145-155.

Hirth, J. P. and Lothe, J. (1992), *Theory of Dislocations*, Krieger Publishing Company.

Kato, M. (1999), *Introduction to the Theory of Dislocations*, Shokabo, Japan.

Kimura, K., Kushima, H. and Abe, F. (2003), "Improvement of creep life prediction of high Cr ferritic creep resistant steels by region partitioning method of stress vs. time to rupture diagram", *J. Soc. Maters. Sci. Japan*, **52**-1, 57-62.

Kubin, L. P., Canova, G., Condat, G., Devincre, B., Pontikis, V. and Brechet, Y. (1992), "Dislocation microstructures and plastic flow: 3D simulation", *Solid State Phenomena*, **23** & **24**, 455-472.

Kushima, H, Kimura, K. and Abe, F. (1999), "Degradation of Mod.9Cr-1Mo steel during long-term creep deformation", *Tetsu-to-Hagane*, **85**-11, 841-847.

Maruyama, K., Sawada, K. and Koike, J. (2001), "Strengthening mechanisms of creep resistant tempered Martensitic Steel", *ISIJ International*, **6**, 641-653.

Taneike, M, Kondo, M. and Morimoto, T. (2001), "Accelerated coarsening of MX carbonitrides in 12%Cr steels during creep deformation", *ISIJ International*, **41**, Supplement, S111-S115.

Zbib, H. M., Rhee, M. and Hirth, J. P. (1998), "On plastic deformation and the dynamics of 3D dislocations", *Int. J. Mech. Sci.*, **40**, 113-127.

Zbib, H. M. (2002), *Multiscale Dislocation Dynamics Plasticity For FCC and BCC Single Crystals Version 02*.